A Novel Approach for the Identification of Material Elastic Constants

Elena Ferretti, Antonio Di Leo and Erasmo Viola

DISTART − Department of Structures Transportations Waters Survey and Territory Engineering, University of Bologna, Bologna, Italy

Abstract The present study is part of an identifying programme for constitutive parameters in damaged materials, termed the "effective parameters". The programme starting point is that the experimental response depends not only on constitutive parameters, but also on structural mechanics and interaction with the test-machine. It is showed how the load-displacement diagram of compressed concrete cylinders is affected by crack propagation, through the resistant structure modification. Moreover, it is analytically demonstrated that the effective stress (σ_{eff})-effective strain (ϵ_{eff}) curve exhibits a strictly positive derivative at the point corresponding to the average stress ($\overline{\sigma}$)-average strain ($\overline{\varepsilon}$) curve peak. Finally, it is proposed a new identification procedure which provided satisfactory results, giving monotone strictly non-decreasing, size-effect insensitive and failure mechanism insensitive $\sigma_{eff} - \varepsilon_{eff}$ curves.

1 Introduction

In order to derive a constitutive law in uniaxial compression from experimental data, it is common practice to define the average stress $\overline{\sigma}$ and the average strain $\overline{\varepsilon}$ as shown in Figure 1. The $\overline{\sigma} - \overline{\varepsilon}$ relationship in Figure 1 is known as uniaxial constitutive law for monotone strain processes. The term "constitutive" is associated with the $\overline{\sigma} - \overline{\varepsilon}$ relationship since this relationship is considered as representative of the mechanic behaviour of the material. However, one can make the following remarks concerning the choice of this term:-

1. The $\overline{\sigma} - \overline{\varepsilon}$ law in Figure 1 is size−effect sensitive, while a constitutive law should not exhibit a size effect.
2. The identification procedure in Figure 1 consists of a mere change of scale. Thus, experimental and identified curves are homothetic (Figure 1). In particular, they both exhibit a softening behaviour. Nevertheless, it is not possible to associate a physical meaning with the softening behaviour of a material response, as the concept of instability loses its sense in the infinitesimal neighbourhood of a point (Ferretti, 2001). Strain−softening has been widely regarded as inadmissible by several authors (Bazant et al., 1997), from the beginning of the 20th century forth.

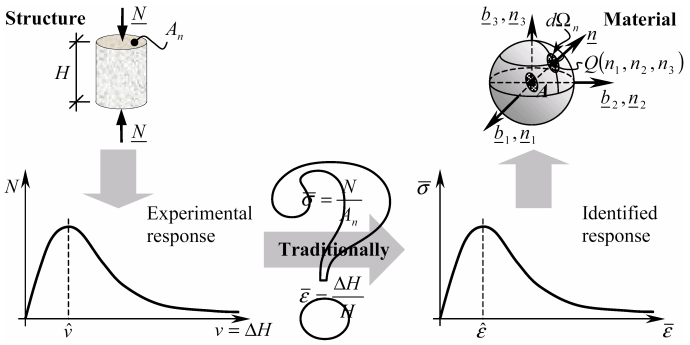

Figure 1. Traditional identification of mono-axial constitutive law by experimental tests.

These inconsistencies come from the impossibility of performing mechanical tests on the material directly: the object in testing is never the material, but a structure interacting with the test−machine (Figure 1, (Ferretti et al., 1999)). Thus, experimental results univocally characterise the behaviour of the specimen−test machine system, while they are not at all representative of the behaviour of the material. In particular, the softening branch has a meaning that is only linked to the structural instability. This branch cannot provide information on the constitutive behaviour, but through an identifying model. To this aim, the evaluation of all factors influencing a test result is needed. Indeed, since the specimen is a structure, experimental results (R) depend not only on constitutive properties (C), but also on structural mechanics (S), interactions between test−machine and specimen (I), and test−machine metrological characteristics (M):

$$R = C + S + I + M. \tag{1.1}$$

It is then necessary to define an identifying procedure from experimental data to material behaviour (inverse problem), which is not affected by the remarks concerning the approach in Figure 1. On the base of partially analogous considerations, Rosati and Natali Sora (2001) have recently proposed a complete response for tensioned concrete.

2 Identification Approach of the Mono-Axial Effective Behaviour

2.1 Identification of the Effective Stress

Name K_C, K_S, K_I, and K_M the weighed contributions assumed by C, S, I, and M, respectively, in the definition of R (Eq. 1.1):

$$C = K_C R, \quad S = K_S R, \quad I = K_I R, \quad M = K_M R. \tag{2.1}$$

From Eqs. 1.1 and 2.1, it follows that $K_C + K_S + K_I + K_M = 1$. All the contributions but the constitutive behaviour can be grouped in one factor K:

$$K = K_S + K_I + K_M. \tag{2.2}$$

From the identifying procedure in Figure 1 it follows that:

$$C \equiv R. \tag{2.3}$$

With the positions in Eqs. 1.1, 2.1 and 2.2, the Eq. 2.3 is replaced by the relationship:

$$C = (1 - K)\, R. \tag{2.4}$$

Eq. 2.4 allows evaluation of the constitutive properties, taking into account the behaviour of the specimen−test machine system. This approach is formally more correct than the approach in Eq. 2.3. Nevertheless, it is not of immediate use, since $K_C = K_C(R)$, $K_S = K_S(R)$, $K_I = K_I(R)$, and $K_M = K_M(R)$ are load−step functions. Then,

$$K = K(R) \tag{2.5}$$

is a load−step function, and not a constant of the performing test. In conclusion, it is not possible to establish a homothetic correspondence between the experimental load−displacement and the uniaxial stress−strain relationship. Moreover, since Eq. 2.5 is not of objective determination, K can only be estimated, with regard to the material scale. This involves the identification of an effective and not constitutive response.

The loss of homothetic behaviour allows us to obviate to the second remark in §1. In other words, since it is impossible to associate a physical meaning with the strain−softening behaviour, we can aspect that the effective laws must be monotone nondecreasing for any material. An analysis of the reciprocal ratios between K_C, K_S, K_I and K_M for compressed concrete cylinders (Ferretti, 2001) showed that $K \cong K_S$: any specimen can be regarded as composed by a resistant structure (Figure 2), in which crack propagation never occurred, and a volume of incoherent material. To identify the scale factor of the σ axis with respect to the N axis (Figure 1), it is then fundamental to introduce a parameter whose dimensions are those of an area and whose incremental law is linked to the structural scheme variation. In the following, this parameter will be termed the resistant area A_{res}. It was here[1] proposed to estimate the resistant area A_{res} in accordance with the Fracture Mechanics with Damage, by means of the damage parameter D (here D has a scalar value):

$$A_{res} = A_n\,(1 - D)\,. \tag{2.6}$$

The effective stress has here been defined as the average stress acting on A_{res}:

$$\sigma_{eff} = \frac{N}{A_{res}} = \overline{\sigma}\frac{A_n}{A_{res}}. \tag{2.7}$$

The analogy with the manner of operation of the Fracture Mechanics with Damage is limited to Eq. 2.6. In the Fracture Mechanics with Damage, D is analytically formulated and considered as uniformly distributed on A_n. In this study, $D = D(R)$ is experimentally evaluated and considered as localised in the volume of incoherent material.

[1] We thank the Italian Ministry for Universities and Scientific and Technological Research (MURST) for its financial support.

Figure 2. Resistant structure at the end of the test.

Algebraic considerations about the formulation of the effective stress. In Eq. 2.7, make explicit the dependence of σ_{eff}, A_{res}, N and D on the displacement v:

$$\sigma_{eff}(v) = \frac{N(v)}{A_{res}(v)}. \tag{2.8}$$

Now, find the derivative of Eq. 2.8 with respect to the variable $\overline{\varepsilon}$:

$$\frac{d\sigma_{eff}}{d\overline{\varepsilon}} = \sigma'_{eff}\frac{dv}{d\overline{\varepsilon}} = H\frac{N'A_{res} - NA'_{res}}{A^2_{res}}. \tag{2.9}$$

The superscript indicates derivation with respect to the variable v, and H is the gage length of $\overline{\varepsilon}$. For the conventions in Figure 1, it follows that:

$$N(v)|_{v=\hat{v}} = N_{\max}, \tag{2.10}$$

where $\hat{v}$ is the value of impressed displacement corresponding to the maximal load. As to the discussion of the sign of Eq. 2.9, it can be stated that:

- N is a monotone nondecreasing function until the peak ($N' \geq 0$, $0 \leq v \leq \hat{v}$), and a monotone strictly nonincreasing function beyond the peak ($N' < 0$, $v > \hat{v}$);
- A_{res} is a monotone nonincreasing function on all the domain ($A'_{res} \leq 0$, $\forall v$), and it can assume a zero tangent only in a neighbourhood of the origin, corresponding to the linear elastic state of the material.

For Eq. 2.6, the assumption of monotonicity for A_{res} involves the monotonicity of the damage law. The experimental results agree with the condition of non zero tangent of A_{res} and D for $v = \hat{v}$, since the crack propagation rate near $v = \hat{v}$ is always very fast:

$$A'_{res}|_{v=\hat{v}} \neq 0, \qquad D'|_{v=\hat{v}} \neq 0. \tag{2.11}$$

It follows immediately that the sign of $d\sigma_{eff}/d\overline{\varepsilon}$ is positive for $0 \leq v \leq \hat{v}$:

$$\frac{d\sigma_{eff}}{d\overline{\varepsilon}} > 0 \qquad 0 \leq v \leq \hat{v}. \tag{2.12}$$

In particular, for $v = \hat{v}$ the Eq. 2.9 assumes the value of:

$$\left.\frac{d\sigma_{eff}}{d\overline{\varepsilon}}\right|_{v=\hat{v}} = -NH\frac{A'_{res}}{A^2_{res}} > 0, \tag{2.13}$$

in which the strict inequality comes from Eq. 2.11. From Eq. 2.13, the first fundamental result follows: a point with strictly positive tangent in the $\sigma_{eff} - \overline{\varepsilon}$ curve corresponds to the point with zero tangent in the $N - v$ curve. This is a notable result, since it has been obtained without having introduced any other assumptions on the shape of the damage law except the condition of non zero tangent in correspondence of the maximal load. The same result for the sign of the tangent can be transposed to the $\sigma_{eff} - \varepsilon_{eff}$ curve, in the point corresponding to the $v = \hat{v}$ point of the $N - v$ curve. The sign of Eq. 2.9 for $v > \hat{v}$ depends on the value of ρ, the ratio between the two terms in the numerator of Eq. 2.9:

$$\rho = \frac{N' A_{res}}{N A'_{res}}; \tag{2.14}$$

$$\frac{d\sigma_{eff}}{d\overline{\varepsilon}} \geq 0 \qquad \forall v > \hat{v},\ 0 \leq \rho \leq 1; \tag{2.15}$$

$$\frac{d\sigma_{eff}}{d\overline{\varepsilon}} < 0 \qquad \forall v > \hat{v},\ \rho > 1. \tag{2.16}$$

In alternative, one can study the sign of the derivative of q, defined as follows:

$$q = \frac{\overline{\sigma}_{\max}}{\sigma_{eff}} \overset{(2.6)}{=} \frac{A_{res}}{A_n} \Big/ \frac{N}{N_{\max}}; \tag{2.17}$$

$$q' = -\overline{\sigma}_{\max}\frac{\sigma'_{eff}}{\sigma^2_{eff}} = -\overline{\sigma}_{\max}\frac{N' A_{res} - N A'_{res}}{N^2}. \tag{2.18}$$

From Eq. 2.18 it can be observed that the sign of q' too is determined by the ratio ρ:

$$q' > 0 \qquad \forall v > \hat{v},\ \rho > 1; \tag{2.19}$$

$$q' \leq 0 \qquad \forall v > \hat{v},\ 0 \leq \rho \leq 1. \tag{2.20}$$

On the other hand, the signs of q' and σ'_{eff} are unconformable $\forall v$ for Eqs. 2.15, 2.16 and 2.18. In conclusion, the sign of $d\sigma_{eff}/d\overline{\varepsilon}$ is surely positive for $0 \leq v \leq \hat{v}$, whereas it is only known when the damage law is known for $v > \hat{v}$. Also this result can easily be transposed to the sign of the derivative of the $\sigma_{eff} - \varepsilon_{eff}$ curve.

2.2 Identification of the Effective Strain

As regards the scale factor of the ε axis with respect to the v axis (Figure 1), the effective strain ε_{eff} has been identified considering that only the conservative forces act in a generic unloading−reloading cycle. In other words, these cycles should be characterised by constant values of resistant area. For this assumption, the instantaneous secant stiffness of the $\sigma_{eff} - \varepsilon_{eff}$ law, $E_s = \tan\alpha$ (Figure 3), is taken equal to the average slope of the unloading−reloading cycle at the current point. Thus, the generic point $\sigma_{eff} - \varepsilon_{eff}$

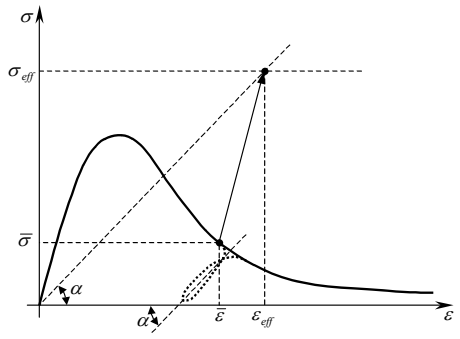

Figure 3. Identification of ε_{eff} starting from the known value of σ_{eff}.

results from the intersection of the two lines $\sigma = \sigma_{eff}$ and $\sigma = E_s\varepsilon$. Figure 3 shows the identification of the effective strain ε_{eff}, starting from the value of effective stress σ_{eff} (Eqs. 2.7 and 2.6) and the knowledge of the damage law D.

3 Sensitivity to the Specimen Slenderness

To operate the transformation in Figure 3 from the $\overline{\sigma} - \overline{\varepsilon}$ diagram to the $\sigma_{eff} - \varepsilon_{eff}$ diagram, the damage law D and the unloading law must be known. In the following, a proposal to experimentally evaluate these laws is presented.

The results on six geometries of cylindrical concrete specimens, with the height−radius ratio variable between three and eight (Ferretti, 2001), will be here presented. Three specimens have been made for each of the six geometries. All the eighteen specimens have been tested in monotone uniaxial load, in the same thermo−hygrometric and curing conditions.

3.1 Unloading Law

The Figure 4 shows how the unloading law is sensibly independent on the slenderness of the specimens. This result supports the assumption for which all the parameters characterising the unloading−reloading cycles, included their average slope, are linked to proprieties of the material and do not depend on the structural mechanics. This happens since the resistant area does not change in the unloading−reloading cycles.

3.2 Experimental Damage Law

To evaluate $D = D(R)$, two experimental damage laws were employed. The first damage law, D_1 (Daponte and Olivito, 1989), relates the damage to the percentage variation of the microseismic signal velocity V at the current point (set−up of the microseismic test in Figure 5.a):

$$D_1 = 1 - V/V_0, \tag{3.1}$$

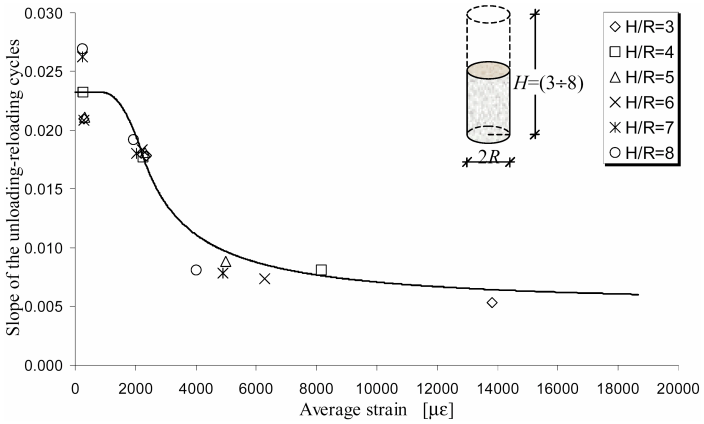

Figure 4. Interpolating law of the unloading-reloading cycles average slope variation for variable slenderness.

where V_0 is the initial microseismic signal velocity. The second damage law, D_2 (Ferretti et al., 1999), relates the damage to the dissipated energy W_d at the current point (Figure 5.b):

$$D_2 = W_d / W_{d,t}, \tag{3.2}$$

where $W_{d,t}$ is the total dissipated energy. D_1 and D_2 turned out to be very close to each other (Ferretti, 2001), until the acceptability threshold of the added noise. This threshold corresponds to the value of deformation beyond which the noise of the crack propagation disturbs the microseismic survey so much that the variations of the microseismic signal cannot be appreciated any longer. For Eq. 2.6, the D_1 and D_2 damage values can be seen in Figure 6 as the one's complement of the percentage resistant area. Only the D_2 damage law has been used in the following, since it has no limitations in the survey field.

The assumption of only conservative forces acting on the unloading−reloading cycles allows evaluation of the specimen defects at the natural state, through the initial damage D_0 (Ferretti and Carli, 1999). In this assumption, indeed, D_0 comes from the ratio

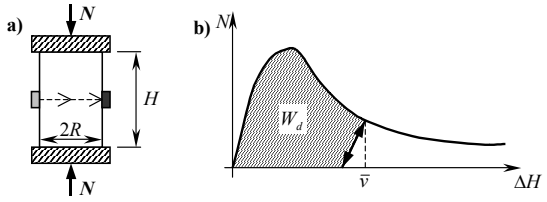

Figure 5. a) Test set-up for the acquisition of D_1; b) Evaluation of W_d.

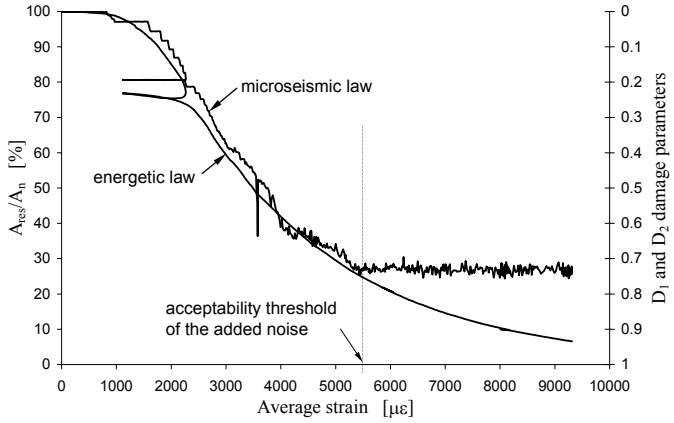

Figure 6. Comparison between the energetic and microseismic laws.

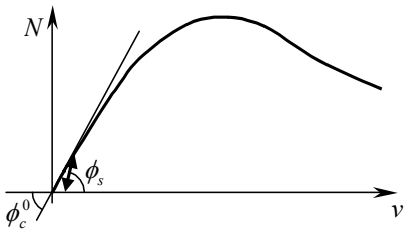

Figure 7. Parameters used to evaluate initial damage D_0 .

between the slope of the stabilising cycle and the tangent to the origin of the $N - v$ diagram (Figure 7):

$$D_0 = 1 - \frac{E^0(\varepsilon)}{E^0_{eff_1}(\varepsilon)} \cong 1 - \frac{\tan\phi_c^0}{\tan\phi_s^0}. \tag{3.3}$$

It must be incidentally recalled that a stabilising cycle is an unloading−reloading cycle that is effectuated for a preloading equal to about the 10% of the maximal presumed load. The stabilising cycle is done in order to limit the influence of the specimen−test machine interaction and test−machine metrological properties on the result. The moderate value of the preloading and the mechanical meaning of the unloading−reloading slopes allow one to associate the difference between the loading and unloading slopes with a damage that is load history independent, characterising the specimen at the natural state.

In accordance with Eq. 3.3, Eq. 2.6 has been modified as follows:

$$A_{res} = A_n(1 - D_{eq}). \tag{3.4}$$

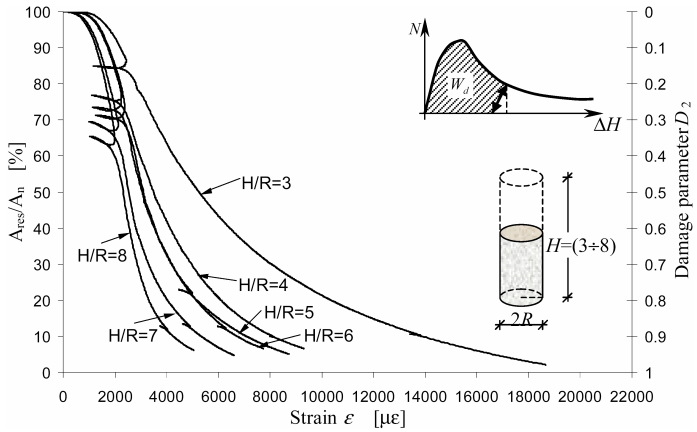

Figure 8. Evolution of resistant area and D_2 damage law for variable slenderness.

D_{eq} is the equivalent damage, comprehensive both of the initial damage D_0 and the damage D_2 due to the monotone loading. D_{eq} can be expressed as:

$$D_{eq} = 1 - (1 - D_0)(1 - D_2) = D_0 + D_2 - D_0 D_2. \tag{3.5}$$

The nominal area deprived of the defects at the natural state, termed the reduced nominal area A'_n, results from:

$$A'_n = A_n (1 - D_0). \tag{3.6}$$

Damage laws were experimentally derived for variable specimen slenderness. The Figure 8 shows the D_2 damage laws obtained for H/R ratios varying from 3 and 8. As can be seen in Figure 8, damage laws are size−effect sensitive. That is, the highest is the H/R ratio, the highest is D for every load−step.

3.3 Sign of the Effective Stress Derivative

As previously stated, the damage can be seen in Figure 9 as the one's complement of the percentage resistant area. The derivative of the experimental damage law in Figure 9, D', turned out to be very close to assume a maximum for $v = \hat{v}$. This result validates the assumption in Eq. 2.11, and corresponds to a fast crack propagation situation.

As regards the sign of the effective stress derivative after the peak, the experimental $q(v)$ function turned out to be a positive−valued, monotone strictly nonincreasing function (Figure 10). The discussion on D' is independent on the single test, and the behaviour in Figure 9 for $v = \hat{v}$ can be generalised. Indeed, the adopted damage law (Eq. 3.2) has a shape that is widely determined by the integral of the $N - v$ curve. Hence, since the $N - v$ curve exhibits a maximum for $v = \hat{v}$, the damage law assumes its maximum derivative in the neighbourhood of $\hat{v}$:

$$q'(v) < 0 \qquad \forall v. \tag{3.7}$$

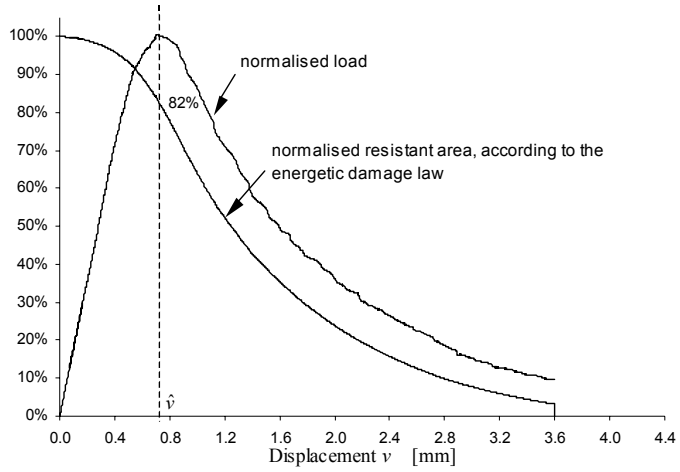

Figure 9. Comparison between the load and resistant area normalised laws.

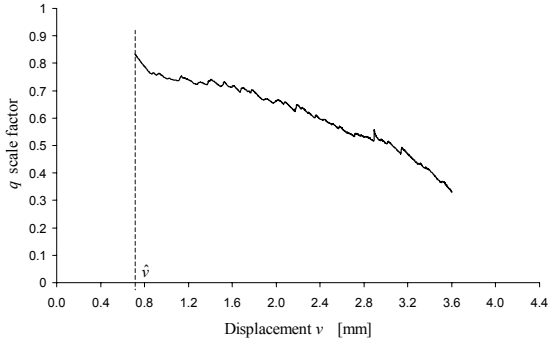

Figure 10. Scale factor between the percentage resistant area and normalised load laws.

This implies that the resistant area decreasing rate was faster than the load decreasing rate. This circumstance and the negative sign between q' and σ'_{eff} (Eq. 2.18) ensure the effective stress derivative to be positive also for $v > \hat{v}$.

In conclusion, for the performed experimental programme and the damage law in Eq. 3.2, the effective stress derivative *always* assumes a finite positive value:

$$\frac{d\sigma_{eff}}{d\overline{\varepsilon}} > 0 \qquad \forall v. \tag{3.8}$$

3.4 Effective Curve

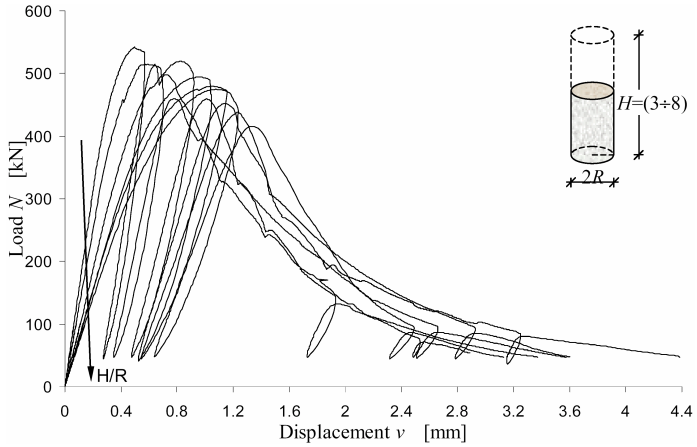

Figure 11. Size effect for the load-displacement diagrams.

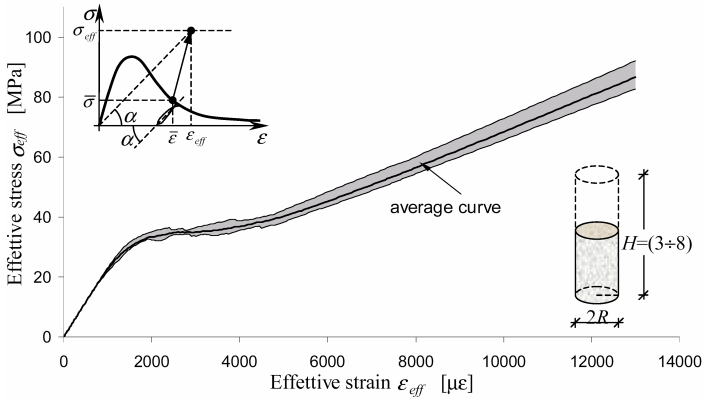

Figure 12. $\sigma_{eff}/\,\varepsilon_{eff}$ dispersion range for variable slenderness and average curve.

The $N-v$ diagrams for the six specimens with varying slenderness (Ferretti, 2001) are shown in Figure 11. In this Figure, the size−effect in the $N-v$ plane involves both a decrement of the tangent to the origin with the increasing of the H/R ratio, and a decrement of the maximum load with the increasing of the H/R ratio.

The $\sigma_{eff}-\varepsilon_{eff}$ relationships obtained for the six tested geometries fall within the grey region in Figure 12 (dispersion range). As previously stated, a strictly positive derivative for the effective properties curves in the $\sigma_{eff}-\varepsilon_{eff}$ plane directly follows from the

independence of the behaviour in Figure 9 on the single test. Moreover, it can be stated that the effective properties curves are size−effect insensitive, since the dispersion range is very little. The average curve shape in the $\sigma_{eff} - \varepsilon_{eff}$ plane is representative of the meso−scale material behaviour.

4 Sensitivity to the Failure Mechanism

The results of a second experimental programme are presented, as to provide a further validation to the proposed identification procedure. Also this experimental programme was performed in the intent to derive a qualitative and not quantitative information. For this reason, the number of the specimens was limited to two. This second time, the geometry of the two specimens is the same, but they are forced to fail in different ways.

As well known, a concrete cylinder in uniaxial compression fails with a dominant bi−cone shaped crack which enucleates in correspondence of the press plates and propagates towards the middle cross−section (Figure 13). To modify the failure mechanism, one of the two specimens was cut along its middle cross−section. Before restoring the specimen, three grommets were fixed on the middle cross−section (Figure 13). The restoration of the specimen has been carried out with mortar. Since the stiffness of the grommets is much higher than the stiffness of the concrete, once loaded the specimen the three grommets have the function to concentrate the load in correspondence of their fixing points. This results in a failure mechanism with the dominant crack enucleating on the middle cross−section, starting from the fixing points of the grommets (Figure 13). The final failure surfaces were the same in the two cylinders (Figure 13).

In Figure 14 the load−displacement experimental curves for the uncut and the cut cylinder are shown. Theese curves are almost superimposed as long as the dominant crack does not start to propagate. That is, the initial stiffness of the restored specimen is almost the same as the initial stiffness of the uncut specimen, stating that the cut and the subsequent restoring have not significantly modified the cylinder stiffness properties.

When the dominant crack starts to propagate, the two curves bifurcate, assuming a different shape (Figure 14). The presence of a bifurcation point confirms that the failure mechanisms of the two specimens were actually different, as it was in the Authors aims.

In Figure 15, the percentage difference from the mean value of load is quoted for intervals of displacement of 0.08 mm. The two local maximums are quoted on the plot.

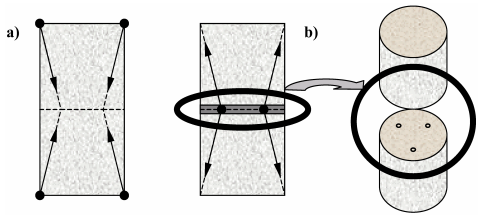

Figure 13. Crack path for the uncut (a) and the cut (b) cylinder.

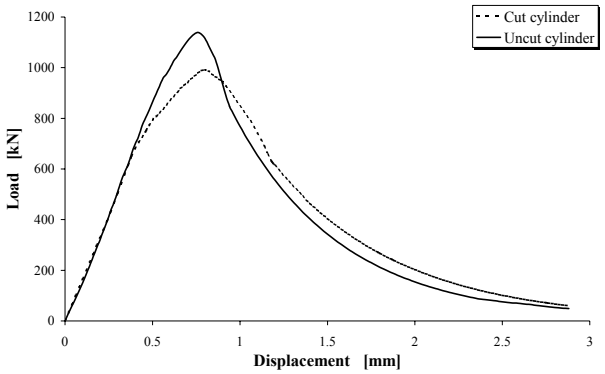

Figure 14. Load-displacement curves for the cut and the uncut cylinder.

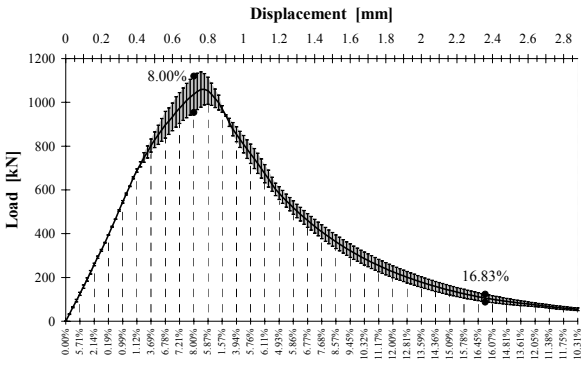

Figure 15. Percentage difference from the mean value of load, at intervals of displacement of 0.08 mm.

The maximum percentage difference from the mean value is reached in advanced phase of softening (Figure 15) and is equal to about 17%. The maximum percentage difference in the neighborhood of the peak is equal to about 8% (Figure 15).

Evaluation of the damage laws D_1 and D_2 has been carried out in accordance with Eqs. 3.1 and 3.2, giving very close results until the acceptability threshold of the added noise this second time too. The initial damage D_0 and the equivalent damage D_{eq} have been identified, respectively, in accordance to Eqs. 3.3 and 3.5, with the reduced nominal area A'_n given by Eq. 3.6. The experimental $q(v)$ function turned out to be a positive−valued, monotone strictly nonincreasing function and the resistant area decreasing rate was faster than the load decreasing rate, as it was in the first experimental programme.

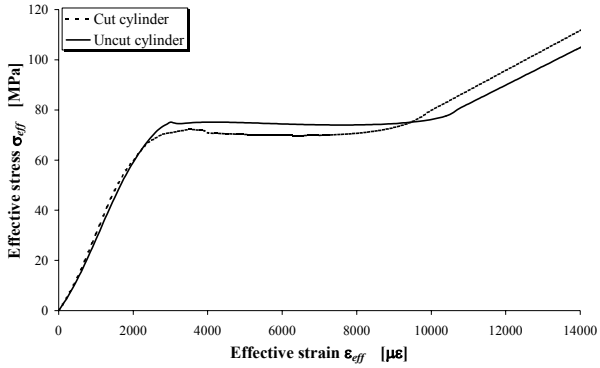

Figure 16. Effective stress-effective strain curves for the cut and the uncut cylinder.

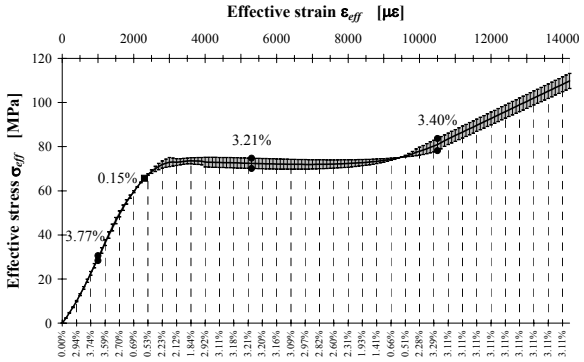

Figure 17. Percentage difference from the mean value of effective stress, at intervals of effective strain of 400 $\mu\varepsilon$.

In Figure 16 the $\sigma_{eff} - \varepsilon_{eff}$ relationships obtained for the two tested cylinders are shown.

In Figure 17, the percentage difference from the mean value of effective stress is quoted for intervals of effective strain of 400 $\mu\varepsilon$. The three local maximums are quoted on the plot. The point of the $\sigma_{eff} - \varepsilon_{eff}$ plane corresponding to the first local maximum in Figure 15 (the point near the peak) is indicated with a square marker. Its percentage difference is quoted on the plot.

As it can be appreciated in Figure 17, the percentage difference from the mean value computed in the $\sigma_{eff} - \varepsilon_{eff}$ plane is noticeably lower than the percentage difference from the mean value computed in the $N - v$ plane.

5 Conclusions

Considering the specimen as a structure interacting with the test−machine, it was demonstrated that the $\sigma_{eff}-\varepsilon_{eff}$ curve of damaging materials exhibits a strictly positive derivative at the point corresponding to the peak of the $\overline{\sigma}-\overline{\varepsilon}$ curve. This result is independent on the adopted damage law.

A procedure to experimentally evaluate the damage law on cylindrical concrete specimens in uniaxial compression has been proposed (first experimental programme). The adopted damage law led to monotone strictly nondecreasing $\sigma_{eff} - \varepsilon_{eff}$ curves for all concrete specimens. Moreover, this curve turns out to be size−effect insensitive.

The two identified $\sigma_{eff} - \varepsilon_{eff}$ curves of the second experimental programme do not exhibit bifurcation points. This means that the identified curve is not sensitive to the change of failure mechanism too. The low value of percentage difference from the mean value in correspondence of the square marker in Figure 17 confirms this conclusion, since for this point the effect of the different failure mechanism reaches a maximum (Figure 15). This result is very important to give validity to the proposed identification procedure, since the independence from the failure mechanism is one of the most important requisites for an identifying procedure of material parameters. Moreover, this result is as much important as the traditional identifying procedure for constitutive laws in uniaxial loading is not insensitive to the change of failure mechanism.

The proposed approach allows identification of a $\sigma_{eff} - \varepsilon_{eff}$ relationship for the description of the meso−scale material behaviour. This relationship, together with adequate failure criteria, leads to structural analysis.

Bibliography

ZP. Bazant, TB. Belytschko and T. Chang. Continuum Theory for Strain-Softening. *Journal of Engineering Mechanics*, 110:1666–1692, 1984.

P. Daponte and RS. Olivito. Crack Detection Measurements in Concrete. In *Proceedings of the ISMM International Conference Microcomputers Applications*, pages 123–127, 1989.

A. Di Leo, A. Di Tommaso and R. Merlari. Danneggiamento per Microfessurazione di Malte di Cemento e Calcestruzzi Sottoposti a Carichi Ripetuti. *Technical note 46, DISTART - University of Bologna - Italy*, 1979.

E. Ferretti. Modellazione del Comportamento del Cilindro Fasciato in Compressione, Ph.D. Thesis: University of Lecce - Italy, 2001.

E. Ferretti and R. Carli. Programma Sperimentale sul Comportamento in Compressione Monoassiale del Calcestruzzo; Parte II: Elaborazione dei Risultati Sperimentali. *Technical note 33, DISTART - University of Bologna - Italy*, 1999.

E. Ferretti, E. Viola, A. Di Leo and G. Pascale. Propagazione della Frattura e Comportamento Macroscopico in Compressione del Calcestruzzo. In *Proceedings of the XIV AIMETA*, on CD-ROM.

G. Rosati and MP. Natali Sora. Tensile Tests on Concretelike Materials: Structural and Constitutive Behaviors. *Journal of Engineering Mechanics*, 127:364–371, 2001.